Materials Advances

ROYAL SOCIETY OF CHEMISTRY

PAPER

View Article Online
View Journal | View Issue

Cite this: *Mater. Adv.*, 2026, 7, 535

Ultrathin boron-doped diamond – surface-wave-plasma synthesis of semi-conductive nanocrystalline boron-doped diamond layers at low temperature

P. Ashcheulov, *[a] M. Davydova,†[ab] A. Taylor,[a] P. Hubík,[a] A. Kovalenko, [c] J. Kopeček, [a] L. Fekete[a] and Z. Weiss [a]

The pursuit of cost-effectiveness has prompted the global scientific community to develop innovative materials and techniques that either meet or surpass essential functionality and performance requirements. In this context, the ongoing development of boron-doped diamond (BDD) electrodes has been demonstrated to significantly contribute to the advancement of several prospective applications, such as electroanalysis, electrosynthesis and electrochemical treatment. Nevertheless, in order for BDD electrodes to compete with inexpensive alternatives, the fabrication of BDD electrodes should be performed in a cost-effective and simple manner. In this work we report on the synthesis of ultrathin boron-doped diamond layers using a surface-wave-plasma (SWP) technique which enables a facile fabrication route for diamond coatings. As SWP synthesis allows for fabrication of BDD at much lower temperatures, when compared to conventional synthesis techniques, ultrathin BDD layers were prepared at 500 °C. A primary focus was given to the systematic optimization of CO_2 concentration in the gas-phase to target BDD layers of moderate semi-conductive electrical characteristics, which are of interest for several applications. Considering the collective research efforts on the development of cost-effective materials and strategies, BDD layers were fabricated in the ultrathin form that supports not only the reduction in fabrication time and energy consumption, but also offers a versatile functional material that could benefit electro-optical and electrochemical applications.

Received 17th March 2025,
Accepted 18th November 2025

DOI: 10.1039/d5ma00238a

rsc.li/materials-advances

1. Introduction

When it comes to modern technologies across multiple industries, many advancements and breakthroughs have been enabled by the process of miniaturisation, which has played a transformative role in reducing dimensions of various devices and therefore allowing compact, portable, lightweight and energy-efficient alternatives, while minimizing material usage and overall environmental impact. In this context, reducing the dimensions/thickness (from micro down to nanoscale) of known high-performance, but rigid materials (*e.g.*, semiconductors or metals), has been shown to offer several advantages in terms of properties, such as mechanical flexibility, durability, optical transparency, anti-reflectivity, surface functionalization, anti-fouling and more.[1] Consequently, the development of thin-film variants of various materials allowed the achievement of significant advancements in several key industries (*i.e.*, electronics, optics, healthcare, aerospace) and facilitated the construction of a number of next-generation devices (*e.g.*, soft electronics, biocompatible medical devices).[2]

Several outstanding material characteristics have prompted intensive development and research of synthetic diamond in past decades.[3] Among many superior properties of diamond in particular its robust chemical stability and facile conversion route from a dielectric to an electrical conductor (*via* doping with boron atoms) have contributed to a steady interest in the electrically conductive form of diamond in addressing a variety of interdisciplinary research topics.[4] To date, electrically conductive boron-doped diamond (BDD) electrodes have been extensively practiced in the field of electrochemistry, while multiple other case-studies on the utilization of BDD coatings in bio-sensing, gas-sensing, opto-electronics, and other applications were also reported.[4–9]

Diamond coatings are typically synthesized in the form of thin films (or layers), which are readily deposited onto a

[a] *FZU – Institute of Physics of the Czech Academy of Sciences, Na Slovance 2, 18221 Prague, Czech Republic. E-mail: ashcheulov@fzu.cz*
[b] *Fraunhofer Institute for Applied Solid State Physics, Fraunhofer IAF, Tullastraße 72, 79108 Freiburg, Germany*
[c] *Department of Applied Mathematics, Faculty of Information Technology, Czech Technical University in Prague, Thakurova 9, 160 00 Prague, Czech Republic*
† Current affiliation: Fraunhofer Institute for Applied Solid State Physics, Fraunhofer IAF, Tullastraße 72, 79108 Freiburg, Germany.

number of substrate/support materials (*i.e.*, Si, high-temperature glass, fused quartz, metals). Generally, such films are composed of diamond crystallites/grains of various crystallographic orientations tightly packed in the form of a polycrystalline layer.[3] Depending on the thickness of polycrystalline diamond layers, they are typically classified into microcrystalline (layer thickness above 1 μm) and nanocrystalline layers (composed of smaller grains and of cca 500–1000 nm in layer thickness).[3,10] A vast amount of information regarding electrical, optical, thermal, mechanical and electrochemical properties of microcrystalline form of BDD layers is readily available while many prospective applications have been shown to benefit from the utilization of microcrystalline BDD layers.[11] Nevertheless, it has been demonstrated that certain applications can greatly benefit from the utilization of thin and ultrathin nanocrystalline BDD layers, which in general possess a higher degree of versatility in terms of material properties.[12] As such, optically transparent electrodes, electrochemical sensors, gas-sensors and protective coatings based on thin nanocrystalline diamond layers were recently demonstrated.[13–16]

Fabrication of synthetic diamond (including BDD), in the form of layers, is usually performed using a number of chemical vapor deposition (CVD) techniques, such as hot filament (HF-CVD) or microwave plasma enhanced (MW-PECVD).[17,18] Although at present these CVD techniques are commercially available and have been commonly applied in public and in private research-and-development settings, there are several crucial drawbacks associated with the synthesis process using conventional HF-CVD and MW-PECVD techniques, which in part contributed to hindering of a more widespread adoption and utilization of diamond. In particular, metal contamination of diamond by metal atoms originating from the metal-based filament (in the case of HF-CVD), limited scalability of the deposition area available for the synthesis of diamond (in the case of MW-PECVD) along with the relatively high temperatures (700–1000 °C) limit the type of substrate materials, which can withstand the diamond CVD synthesis. To address the above-mentioned drawbacks of conventional HF-CVD and MW-PECVD synthesis the alternative approaches have been presented. In particular, the distributed antenna array (DAA) and surface-wave-plasma (SWP) MW-PECVD synthesis techniques have been demonstrated for the fabrication of diamond coatings over large areas (wafer-size) and at low synthesis temperatures (down to 250–300 °C).[19–24] Among available CVD alternatives, the SWP-type synthesis system based on linear antennas (MW-LA-PECVD) has been shown to boast several key advantages, such as relatively simple reactor design and overall synthesis-process versatility in terms of deposition parameters, that have stimulated the recent commercial adoption of SWP technique for diamond synthesis (*i.e.*, MW-LA-PECVD).[25]

Recently we have reported on the fabrication of nanocrystalline BDD layers using surface-wave-plasma synthesis in MW-LA-PECVD system.[26] Fabrication of wafer-size BDD films (highly homogeneous BDD coating over 6-inch area) and the synthesis of nanocrystalline BDD layers in the range temperatures (250–750 °C) were demonstrated.[26–28] Additionally, optimization of gas chemistry parameters enabled fabrication of highly conductive (heavily boron-doped) BDD layers in MW-LA-PECVD at 750 °C that possess electrical characteristics similar to that of nanocrystalline BDD layers fabricated using conventional MW-PECVD technique.[27] Despite these achievements, MW-LA-PECVD synthesis of BDD layers exhibiting moderate/semi-conductive electrical characteristics remained largely unexplored. As the BDD layers/electrodes are typically compared in terms of their electrical resistivity characteristic, it has been recently demonstrated that thin-film nanocrystalline BDD electrodes possessing moderate electrical transport properties (*i.e.*, coatings of higher resistivity) can provide additional benefits to various electrochemical processes (*e.g.*, electrochemical reduction of carbon dioxide, oxidative degradation of pharmaceuticals).[29,30]

Given the advantageous characteristics which ultrathin films generally enable due to a reduced thickness (*e.g.*, high optical transparency, certain degree of mechanical flexibility) the current work is aimed at the fabrication of nanocrystalline BDD layers in the ultrathin form using surface-wave-plasma synthesis in MW-LA-PECVD apparatus. Particular focus is given to the synthesis of BDD layers at a low temperature of 500 °C, to fulfill the requirement for a wider selection of substrate materials onto which BDD coatings can be applied. Importantly, as semi-conductive characteristics of nanocrystalline BDD layers fabricated using SWP synthesis in MW-LA-PECVD have not yet been thoroughly investigated, here preparation of ultrathin BDD layers exhibiting moderate electrical characteristics was targeted. Particularly, a systematic optimization of the gas-phase chemistry in terms of addition of carbon dioxide (CO_2) and boron precursors of various concentrations have been performed, as it has been demonstrated that variation of these gas-phase precursors can have a significant effect on the electrical characteristics of BDD layers.[22,27] Furthermore, electrodes based on ultrathin BDD layers were fabricated and investigated for their electrochemical characteristics. Finally, in order to gain insights into ultrathin nanocrystalline BDD layers surfaces, image processing techniques and consequent statistical analysis have been performed.

2. Experimental

2.1 Fabrication of ultrathin nanocrystalline BDD layers

For the surface-wave-plasma synthesis of ultrathin nanocrystalline BDD electrodes a custom-built microwave plasma enhanced CVD reactor with linear antenna delivery (MW-LA-PECVD) was utilized, which is capable of low temperature operation (for more information on the reactor design see ref. 26 and 27). For the fabrication of BDD layers the following substrates were used – electrically insulating high-temperature glass 10 × 10 mm^2 substrates (Corning Eagle XG), quartz, and conductive Si substrates (Si-Mat, Germany, p-type with the resistivity of <0.005 Ω cm, (100)-oriented, 300 μm-thick) cut into 10 × 10 mm^2 pieces. Prior to the synthesis process, all substrates were thoroughly cleaned in an ultrasonic bath using acetone, isopropyl alcohol, mixture of H_2SO_4/H_2O_2 and eventually rinsed in deionized water. In the case of Si substrates an additional

treatment step (in HF acid) has been performed to remove the SiO_2 native layer, to prevent formation of highly resistive interface between Si and nanocrystalline BDD layer. To create an initial layer of diamond nuclei/particles for the consequent growth of these particles into crystals, substrates were seeded with nanodiamond dispersion (NanoAmando, from NanoCarbon Institute-Japan) in water (0.2 g L^{-1}) using spin coating.

For the growth of nanocrystalline BDD layers the $H_2/CH_4/B_2H_6/CO_2$ gas admixture was implemented, which is typical for the synthesis of boron doped diamond using the MW-LA-PECD system.[27] Diborane gas (B_2H_6, 7500 ppm in H_2) was used as a boron precursor, while the range of B/C ratios in the gas-phase (further referred in ppm) was chosen as 60 000 (also referred as 60k), 6000 (also referred as 6k), 600 and 60. The implemented synthesis/deposition parameters are listed in Table 1. During the synthesis process the temperature at the surface of substrates was monitored *via* a Williamson Pro 92-38 infrared pyrometer, while the temperature of the substrate holder was monitored *via* thermocouple mounted directly into the holder. Generally, depending on the substrate holder configuration (heated *via* applied high-voltage/unassisted/water-cooled) the synthesis in the MW-LA-PECVD system can be performed within the range of temperatures, typically at 750, 550 and 250 °C, respectively.[28,29] Here, the low temperature synthesis of nanocrystalline BDD layers was performed in the unassisted configuration of the substrate holder, where the recorded temperature peaked at cca 500 °C. Such a temperature is reached *via* the heat from the generated plasma. The growth process duration was set to 6 hours for each deposition cycle to allow for comparison between the layers. Importantly, as it has been demonstrated in our earlier studies on diamond synthesis in the MW-LA-PECVD system, the addition of CO_2 in the gas-phase is essential for the suppression of SiC, which can be formed due to the presence of Si species in the plasma originating from the etching effect of quartz tubes, which are located inside the growth chamber.[27] Therefore, in this work the zero concentration of CO_2 was omitted, and the range of CO_2 concentrations (in %) in the gas-phase was chosen as 0.1, 0.5, 1, 1.5 and 2% (see Table 1 for details).

2.2 Characterization of ultrathin nanocrystalline BDD layers

BDD layers deposited onto insulating glass substrates were subjected to Raman spectroscopy analysis and electrical characterization, while samples deposited onto conductive Si substrates were used for the evaluation of surface morphology/layer thickness and boron incorporation characterization. Raman spectroscopy analysis was carried out at room temperature using a Renishaw InVia Raman Microscope under a laser excitation wavelength of 488 nm with the laser power at the sample of 6 mW, ×50 Olympus objective, 65 mm slits, spot focus and grating of 2400 lines per mm. A high pressure high temperature single crystal diamond (Ib) was used as a reference for the sp^3 Raman peak position. The spectrometer was calibrated by the F1g mode of silicon at 520.2 cm^{-1}.

The surface morphology of nanocrystalline BDD layers was then analyzed by scanning electron microscopy (SEM) using a Tescan FERA 3 GM system. Particular attention was given to the evaluation of thickness of deposited layers using SEM – firstly, each examined BDD sample (on Si substrate) was synthesized at the exact same position on the substrate holder to account for any plasma inhomogeneity due to placement of the antennas above the substrate holder (see ref. 27 for more details). After synthesis, each BDD sample was cut into two pieces which underwent cross-sectional SEM measurements at several points along the performed cut to collect information on the thickness of layers.

To complement the data on surface morphology and to obtain information on the surface roughness of fabricated BDD layers (on Si), atomic force microscopy (AFM) measurements were performed using Dimension ICON AFM (Bruker) operating under ambient conditions. AFM images were obtained by the Peak Force Tapping mode using Tap150AL-g probes. Images with areas of 5 × 5 μm^2 were collected with 512 × 512 points per image.

For electrical characterization triangle contacts (Ti-20 nm/Au-100 nm) were evaporated onto four corners of BDD coated square glass substrates. Consequently, electrical resistivity was measured by the differential van der Pauw (vdP) method at room temperature using a Keithley 6221 current source and two electrometers (Keithley 6514) with a Keithley 2182 A nanovoltmeter which recorded the voltage difference between the electrometers, together with a Keithley 708B switching matrix.

To analyse the total boron concentration in samples glow discharge optical emission spectroscopy (GDOES) measurements were performed on BDD coated conductive Si samples. GDOES measurements were performed using a GDA750HR spectrometer (Spectruma GmbH, Germany), with a dc-discharge in argon gas and a 2.5 mm-internal anode diameter Grimm-type spectral source. The optical system of the instrument consists of a f = 0.75 m Paschen–Runge vacuum polychromator with 34 fixed channels with photomultipliers, creating a spectral resolution ≈25 pm. A constant discharge voltage/current of 800 V/15 mA was used in the measurements, voltage was stabilized electronically and current was stabilized by a feedback loop, by adjusting the flow (pressure) of argon. For the calibration certified reference materials (CRMs) of steels and cast irons with known boron and carbon concentrations and known sputter rates were used. The following emission lines of the elements were used for the analysis: C 165 (165.701 nm), B 208 (208.959 nm) and Si 288 (288.158 nm). More details on the GDOES technique and overall analysis procedures can be found in our previous report.[31]

Table 1 Deposition conditions used for synthesis of nanocrystalline BDD layers

H_2 concentration	94–96%
CH_4 concentration	4
CO_2 concentration	0.1–2%
B/C ratio	60–60 000 ppm
Microwave power	2 × 3 kW
Process pressure	0.25 mbar
Substrate temperature	500 °C (±20 °C)
Substrate holder	Unassisted (not water-cooled/not voltage-heated)
Growth/synthesis duration	6 hours

As the morphology of fabricated samples varied from the typical nanocrystalline BDD layers (later discussed in the results section), collected SEM images (top-view) were statistically processed to calculate the distribution of grain sizes on the surface. A visualisation procedure was then performed to outline the contours of diamond grains on the surface. The resulting data provided insights into the uniformity and consistency of the deposition process across different samples. More information on the calculation procedure is detailed in the SI.

Electrochemical characterization of Si/BDD electrodes was performed in a conventional three-electrode set-up, in which a silver chloride electrode (Ag/AgCl, 3 M KCl) and a platinum wire served as reference and counter electrodes, respectively. Cyclic voltammetry (CV) measurements were performed using a Gamry Reference 600+ instrument (Gamry). All electrochemical measurements were performed in 1 M KCl supporting electrolyte at ambient conditions. Redox marker of 1 mM $Fe(CN)_6^{3-/4-}$ (Sigma-Aldrich) in supporting 1 M KCl electrolyte was employed for investigation of charge transfer kinetics. Si/BDD electrodes were placed under circular Teflon-made sealing, such that the top surface of BDD with geometric area of 0.17 cm^2 was exposed to the electrolyte solutions, while electrical contact was provided through the bottom side of conductive Si substrate. Prior to collection of cyclic voltammograms, all examined Si/BDD electrodes were pre-treated in 1 M KCl solution at +3.0 V *vs.* Ag/AgCl for 10 min to ensure replacement of surface hydrogen. CVs were collected at scan rate of 100 mV s^{-1}, while for each tested Si/BDD electrode the 5th CV scan was selected for comparison.

3. Results and discussion

In total, using a low synthesis temperature of 500 °C, 20 samples of ultrathin nanocrystalline BDD layers were fabricated *via* MW-LA-PECVD. BDD layers differed in the amount of utilized CO_2 concentration (from 0.1 to 2% in the gas-phase) and the overall B/C ratio (from 60 to 60 000 ppm in the gas-phase). Table 2 presents details on fabricated nanocrystalline BDD layers and their corresponding physical characteristics.

To understand the effect of the increasing gas-phase CO_2 concentration on the surface morphology of samples, SEM characterization was performed. Fig. 1 presents surface morphologies of BDD layers obtained with different doping levels (B/C of 60 000 ppm and 600 ppm) and various concentrations of CO_2 (0.1, 0.5, 1.5, 2%), while Fig. S1 demonstrates SEM images for all fabricated samples. At first, it is noticeable, that in this case, where ultrathin nanocrystalline BDD layers (thickness of cca. 140–160 nm) have been fabricated at 550 °C, the obtained surface morphology differs from the conventional nanocrystalline morphology where well-developed diamond grains of multiple crystallites orientations are usually present.[27] Here, the overall crystallinity is seen to be less developed, which can be partially attributed to a rather low implemented gas-phase boron concentration, which follows the results reported in previous works.[29] Further, the increase of CO_2 concentration (from 0.1 to 2%) results in the gradual decrease in the size of diamond crystallites for a given gas-phase boron concentration (Fig. 1, and Fig. S1). Such an effect is observed for all employed doping levels (see Fig. S1), indicating that addition of CO_2 in the gas phase affects the morphology of nanocrystalline layers independently of the presence of an additional doping precursor gas (*i.e.* boron).

An additional observation can be made in the case when CO_2 gas-phase concentration is varied particularly in the range of 1.5–2% at lower doping levels (*i.e.* B/C of 600 and 60 ppm) where smaller average size of nanocrystallites (see Fig. S1) are observed, when compared to layers fabricated with higher B/C levels (*i.e.* 6000 and 60 000 ppm). Although the mentioned difference in the gran size (in the case of MW-LA-PECVD synthesis) is not particularly significant due to the overall reduced BDD layer thicknesses (cca 150 nm), it should be

Table 2 Summary of fabricated nanocrystalline BDD samples characteristics

Sample	B/C (ppm)	CO_2 (%)	Thickness (nm)	RMS (nm)	Resistivity (Ohm cm)	B concentration[a] (at. cm^{-3})
BDD-60k-1	60 000	0.1	165	7.6	1.85	7.1×10^{20}
BDD-60k-2	60 000	0.5	167	6.5	4.85	3.2×10^{20}
BDD-60k-3	60 000	1	153	6.4	22.9	2.07×10^{20}
BDD-60k-4	60 000	1.5	155	6.4	24.9	2.3×10^{20}
BDD-60k-5	60 000	2	164	6.4	44.5	6.7×10^{19}
BDD-6k-1	6000	0.1	147	6.6	87	2.6×10^{20}
BDD-6k-2	6000	0.5	155	6.7	670	2.07×10^{20}
BDD-6k-3	6000	1	155	6.5	878	2.3×10^{20}
BDD-6k-4	6000	1.5	154	6.5	3094	2.4×10^{20}
BDD-6k-5	6000	2	148	6.2	11 109	3.4×10^{20}
BDD-600-1	600	0.1	140	6.4	1450	1.3×10^{20}
BDD-600-2	600	0.5	144	6.7	4145	1.5×10^{20}
BDD-600-3	600	1	140	6.7	19 340	1.41×10^{20}
BDD-600-4	600	1.5	149	7.6	94 500	1.21×10^{20}
BDD-600-5	600	2	158	7.2	81 070	1.82×10^{20}
BDD-60-1	60	0.1	139	6.8	8580	9.4×10^{19}
BDD-60-2	60	0.5	142	6.8	54 610	6.07×10^{19}
BDD-60-3	60	1	124	6.6	114 500	1.12×10^{20}
BDD-60-4	60	1.5	137	6.4	134 700	1.1×10^{20}
BDD-60-5	60	2	142	6.6	303 500	1.8×10^{20}

[a] Boron concentration estimated from GDOES measurements.

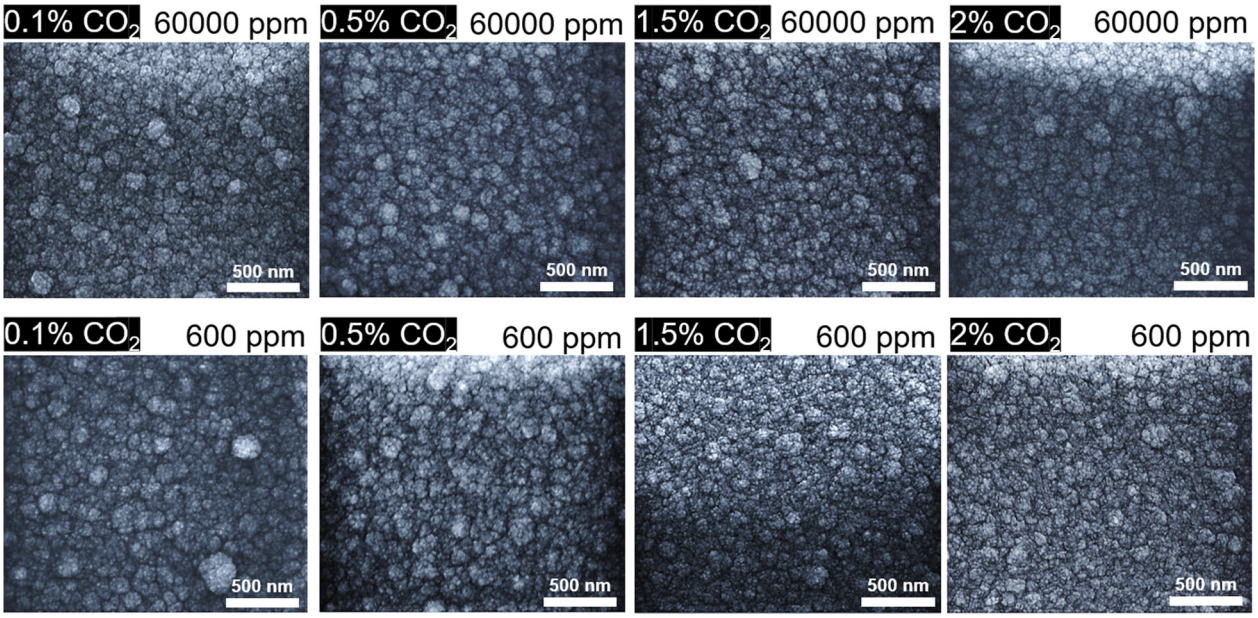

Fig. 1 Top-view SEM images of ultrathin boron-doped diamond layers fabricated at 500 °C with B/C of 60 000 and 600 ppm and with the gas-phase CO_2 concentrations of 0.1, 0.5, 1.5, and 2% demonstrating the gradual decrease in the size of diamond crystallites with the increasing CO_2 gas-phase concentration.

noted, that the observed trend is different to the one previously reported for the conventional MW-PECVD growth where the increase of the gas-phase boron concentration resulted in the decrease of grain size.[27] Nevertheless, the above-mentioned observations are in line with our previous reports, and can be ascribed to the contrasting growth conditions during MW-PECVD and MW-LA-PECVD synthesis.[29] Overall, results of the SEM characterization supports previously reported observation on the presence of oxygen (in the form of CO_2 gas) during synthesis of nanocrystalline diamond layers in MW-LA-PECVD, where improvements in the layers crystallinity have been demonstrated and attributed to the CO_x species in the plasma and their influence on the abstraction/etching rates of atomic H that provides stabilization of sp^3 bonds on the forming diamond crystallites.[26,32] It should be noted that any further increase in the CO_2 concentration (above 2% in the gas phase) is expected to drastically suppress boron incorporation (further discussed in the text) along with the formation of "platelet"-type surface morphology (*i.e.*, prolonged and faceted grains) which may cause formation of pinholes in the layers.[33]

Taking into account the observed deviation of the surface morphology (see Fig. 1 and Fig. S1) from the typical morphology consisting of well-developed diamond grains, estimation of grain sizes for fabricated ultrathin BDD layers is rather complicated. Therefore, image processing techniques, to extract the size distribution of the grains, have been implemented. SEM images were denoised, binarized using Otsu threshold,[34] and then the equivalent circular diameter was calculated for each particle (assuming that the particles are on average circular) after detecting the contours of the binary particles. A detailed description of the implemented technique can be found in the SI file. Fig. 2(a) demonstrates the SEM image of BDD-6k-1 sample with the superimposed layer of contours (shown in green color), which define the calculated boundaries of individual grains. It is worth noting that although not every diamond grain was defined/contoured by the algorithm (where results were dependent on the overall quality of the acquired SEM image – see SI for details) the resultant data allows for the statistical analysis and estimation of the grain size distribution for each fabricated nanocrystalline BDD layer (characterized by SEM). Fig. 2(b) demonstrates calculated distribution of grain sizes for BDD-6k-1 sample, where the equivalent diameter of algorithmically defined grains is plotted as a function of frequency when a particular grain-size is detected. Fig. S2 presents calculated grain size distribution results for all fabricated BDD layers where the prevalence of small grains (below 50 nm in diameter) is discernible for all samples. Furthermore, BDD layers prepared with lower B/C ratios (*e.g.*, 60 ppm) and higher CO_2 concentrations (1.5–2%) exhibit the occurrence of very small grain-sizes, down to the equivalent diameter of 20 nm (see Fig. S2), once again confirming the observations made *via* the SEM analysis and highlighting the effect of boron addition on the slight improvement of the diamond growth/grain-size formation (in MW-LA-PECVD).

By establishing an equal duration for all growth processes (6 hours) the comparison between fabricated BDD layers thicknesses along with the estimation of growth rates for a given gas-phase parameters (CO_2 concentration and B/C ratio) has been performed. Accordingly, Table 2 summarizes growth rates and measured thickness data (collected *via* SEM) for samples with different gas-phase CO_2 concentrations and B/C ratios. At first, variation of the CO_2 gas-phase concentration has a rather insignificant effect on the overall BDD layer thickness, where only negligible changes (within cca ±20 nm) from an average

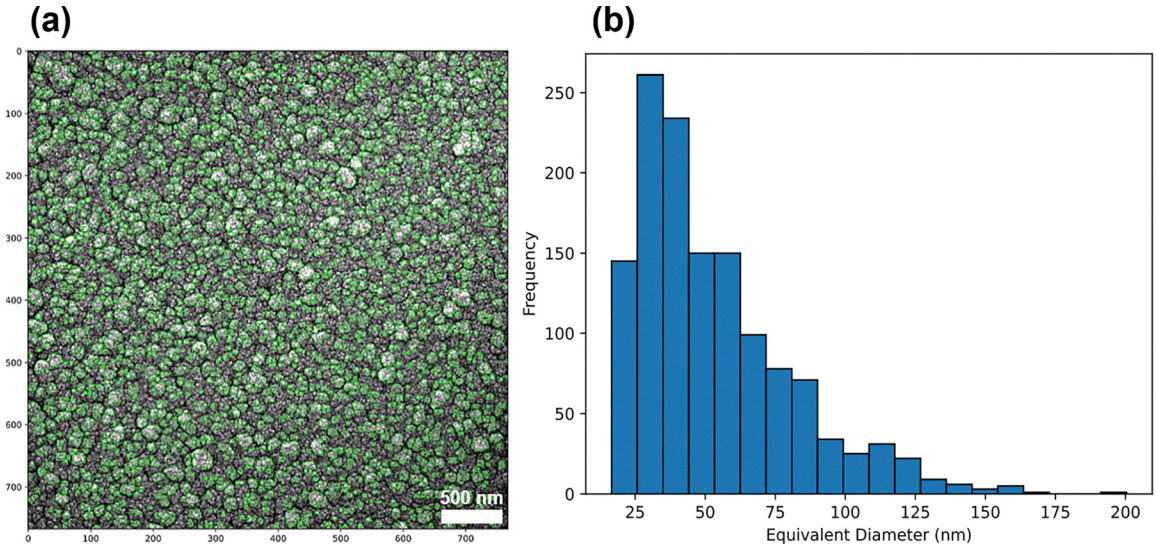

Fig. 2 (a) SEM image of the BDD-6k-1 layer with the superimposed layer of contours (in green color) that define the diamond grains. (b) Grain size distribution calculated for the BDD-6k-1 layer using image processing.

thickness of 150 nm are visible (see Fig. 3(a)). The BDD layers fabricated with B/C of 60 000 ppm (BDD-60k) exhibit the highest thickness (reaching 165 nm) amongst obtained sample batches, while samples with B/C of 6000 ppm (BDD-6k) demonstrate slightly smaller average thickness of 150 nm (see Fig. S3 for SEM cross-section thickness measurement). Consequently, BDD layers prepared with a lower B/C ratios of 600 and 60 ppm (*i.e.*, BDD-600-1,2,3,4 and BDD-60-1,2,3,4) exhibit even lower thickness values reaching cca 130 nm (Fig. 3(a)), although a small uptrend in thickness variation is visible at higher CO_2 concentrations (up to cca 160 nm). Such a result can be partially ascribed to the presence of boron species (along with H from the B_2H_6 precursor) in the gas admixture which can slightly accelerate the growth process when compared to boron-free gas chemistries (*i.e.*, $H_2/CH_4/CO_2$); however, further detailed studies are required to fully understand this observation.

Furthermore, since the low temperature synthesis was targeted in this work, the growth rate values, which present an important aspect in the fabrication of BDD layers, were additionally estimated. The resultant growth rates are seen to be below 30 nm h^{-1} in the case of all fabricated layers, and given that the corresponding values were calculated from the thickness data, the growth rates follow a similar trend in regards to implemented B/C ratios and CO_2 concentrations (see Fig. 3(b)). Implementing higher B/C ratios results in higher growth rates, which goes in line with our previous report.[26,27]

To complement SEM measurements, AFM characterization was performed, and the typical AFM image of ultrathin BDD layer (sample BDD-60k-1) is demonstrated in Fig. 4(a), while

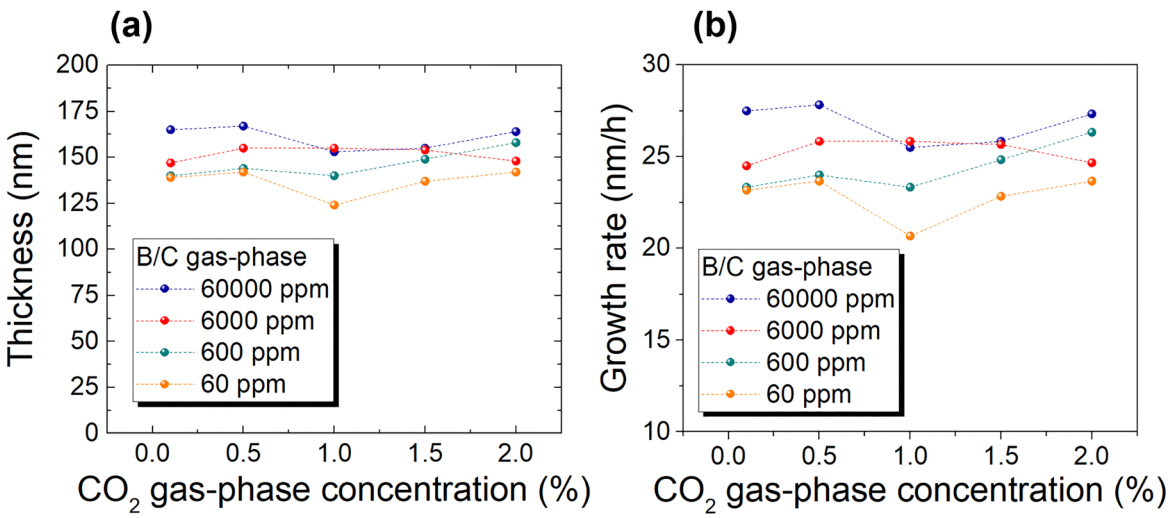

Fig. 3 (a) Thickness data for ultrathin nanocrystalline BDD layers as a function of the B/C ratio and gas-phase CO_2 concentration, as calculated from the cross-section SEM examinations. (b) Growth rate values for the synthesis of BDD layers in MW-LA-PECVD system.

results for all samples are presented in Fig. S4. Overall, the surface morphology of nanocrystalline BDD layers as characterized *via* AFM imaging demonstrates similar features observed in SEM analysis (Fig. 1) – the presence of small diamond grains with no clear faceted structures, along with the appearance of larger clusters for layers fabricated with higher B/C ratios (6k and 60k ppm).

An additional advantage of ultrathin films and specifically nanocrystalline form of diamond layers is that corresponding surfaces are usually smooth (nm scale) which could provide a benefit for many potential applications. Particularly, a higher degree of surface smoothness would be beneficial for optoelectronic applications of ultrathin BDD layers, as smooth surfaces usually minimize light scattering and enable direct light transmission.[9] Our earlier works detailed the optical properties of BDD layers, reporting transmittance as a function of the B/C gas-phase ratio, layer thickness, and CO_2 concentration. The gradual increase of the B/C ratio in the gas-phase (*i.e.*, the increase in the boron concentration in the solid phase) has contributed to the reduced levels of optical transmittance for cca 150 nm thin BDD layers (down to 50% in the visible part of the spectrum).[13] Similarly, the optical transmittance was seen to exhibit reduced values (below 50%) for thicker BDD films (cca 300 nm and above).[28] Furthermore, the increase in the CO_2 addition in the gas-phase resulted in the improvement of transmittance values attributed to the lesser degree of non-diamond content incorporation in BDD layers at higher CO_2 concentrations.[35]

In this regard the fabricated BDD layers were further characterized to examine the surface characteristics, specifically surface roughness (*via* AFM). Measured values of surface roughness (RMS) are presented in Table 2, and their variation depending on the implemented levels of B/C and CO_2 in the gas phase are demonstrated on Fig. 4(b). Due to their relatively low thickness, samples exhibit smooth surfaces with RMS roughness values between cca 6 and 8 nm. Typically, thicker nanocrystalline diamond layers (*i.e.* above 500 nm) will exhibit higher RMS values (20–30 nm) due to more developed diamond grains. Additionally, as seen from Fig. 4(b), the variation of the gas-phase parameters (B/C and CO_2) has an insignificant impact on the evolution of the surface roughness, which is also supported by the SEM observations mentioned above. Finally, estimation of the BDD layers thickness using AFM technique (see Fig. S5) provided comparable values as measured *via* SEM cross-sectional examination.

To characterize the quality of the fabricated ultrathin nanocrystalline BDD layers, Raman spectroscopy measurements were performed. All fabricated samples demonstrate the presence of a sharp diamond-related peak located at around 1322–1331 cm^{-1} (Fig. 5(a)–(d)), highlighting the successful diamond synthesis process at rather low temperatures (500 °C). It is worth noting that, due to the rather low utilized boron-doping levels in the gas-phase (B/C of 60k ppm and lower) the peaks typically associated with the boron-doping effect (*e.g.*, at 1230 and 500 cm^{-1}) are absent in the spectra (see Fig. S), which are usually common for heavily-doped BDD layers (*i.e.*, B/C of 230k ppm) synthesized *via* MW-LA-PECVD technique.[27,29] Despite this fact, for fabricated layers depending on the utilized boron-doping level in gas-phase the diamond peak experiences a slight shift, where for layers doped with B/C ratios of 60 and 600 ppm the peak is located at 1331 cm^{-1}, while for layers doped with 6000 and 60 000 ppm the position of the peak shifts to lower wavenumbers (around 1322 cm^{-1}). Such a shift is primarily associated with an increased concentration of the boron in BDD layers when the B/C ratio in the gas phase is increasing. A further observation can be made in the case of BDD-60k-1 sample (B/C of 60k ppm) where the utilized concentration of CO_2 in the gas-phase was set to a minimum value of 0.1% – an additional distinct peak appears in the Raman spectrum located at around 1210 cm^{-1} which is associated with the maximum of the phonon density of states (PDOS), a typical signature of BDD layers with an elevated fraction of incorporated boron.[29] Nevertheless, due to low

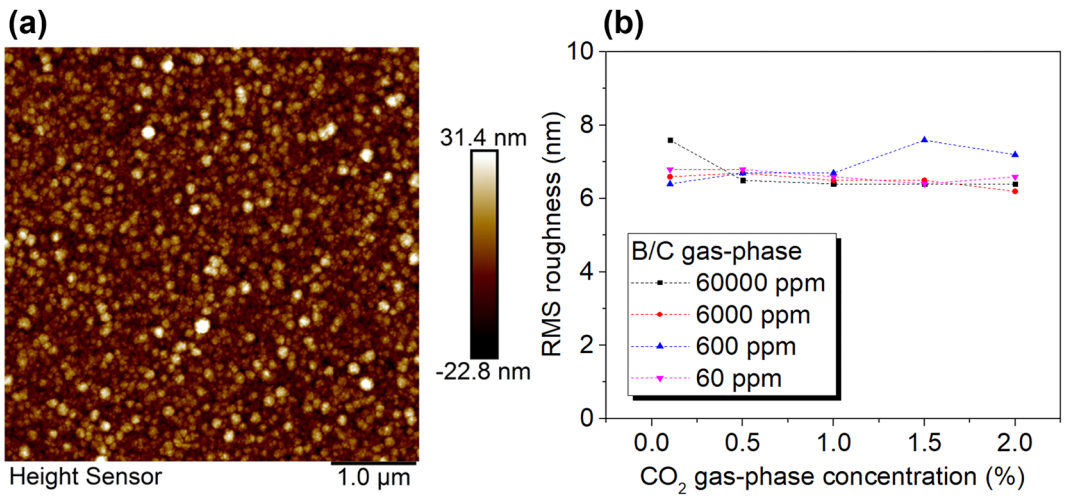

Fig. 4 (a) AFM image collected from the BDD-60k-1 sample showing nanocrystalline character of the surface. (b) Surface roughness (RMS) values as a function of CO_2 gas-phase concentration for BDD layers prepared with various B/C ratios.

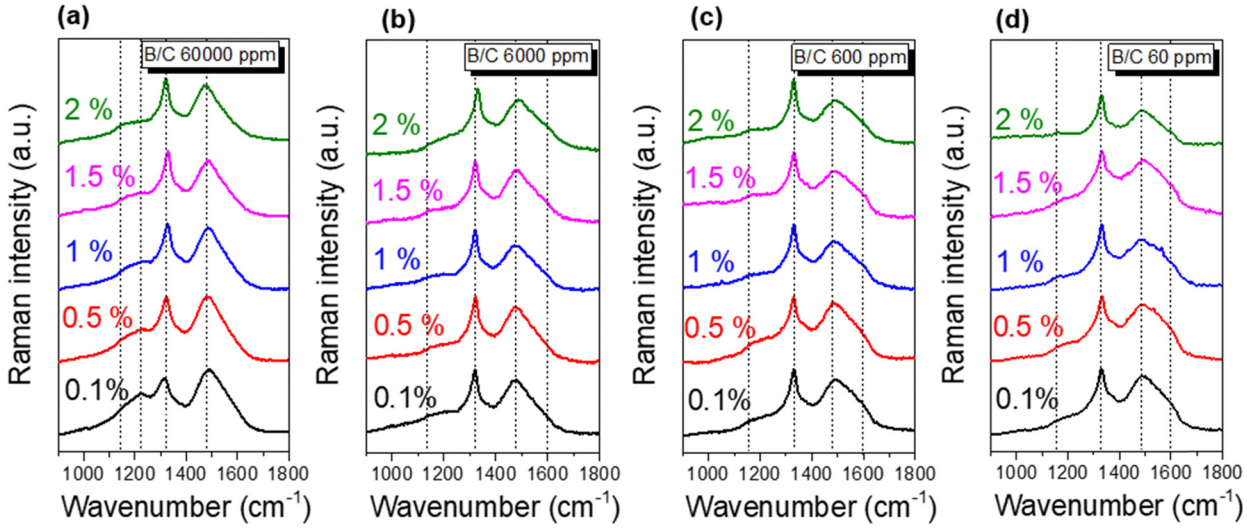

Fig. 5 Raman spectra of fabricated ultrathin nanocrystalline BDD layers with B/C ratios of (a) 60 000 ppm, (b) 6000 ppm, (c) 600 ppm, and (d) 60 ppm. Values of implemented CO_2 gas-phase concentrations are given above each spectrum for a given B/C ratio.

utilized CO_2 concentration (0.1%) the BDD-60k-1 sample exhibits a rather indistinct diamond peak when compared to other samples from the series doped with B/C of 60 000 ppm (Fig. 5(a)) signaling a lesser overall quality of this BDD layer (*i.e.*, decreased sp^3/sp^2 ratio). On the other hand, with an increase in CO_2 concentration (0.5–2%) the intensity of the diamond peak (sp^3-bonded carbon) increases specifically when compared to the intensity of the *trans* poly-acetylene related band centered at around 1480 cm^{-1} (accompanied by a lesser intense band at cca 1150 cm^{-1}). Such an observation supports the previously mentioned observation on the improvement of BDD layers quality with the addition of CO_2 in the gas-phase,[27] while the trend on the increasing intensity of the diamond peak is visible for all herein implemented B/C ratios (Fig. 5(a)–(d)).

Besides the effect of the CO_2 concentration on the improvement of BDD quality, an additional observation can be made when considering the presence of the boron precursor in the gas phase. Nanocrystalline BDD layers synthesized with low B/C ratios (60 and 600 ppm) exhibit formation of an additional band in the Raman spectra located around cca 1590 cm^{-1} known to originate from graphitic structures (planar configuration of sp^2-bonded carbon), which is however suppressed for BDD layers prepared with higher B/C ratios (6000 and 60 000 ppm) (see Fig. 5(c) and (d)). The appearance of the graphitic band in the spectra signals that the incorporation of boron in the gas admixture during BDD layers synthesis in MW-LA-PECVD supports the predominant formation of sp^3-carbon bonds, increasing the overall quality of the layers. Such an observation is important particularly in the context of the ultrathin BDD layers, as due to the nucleation and consecutive growth of diamond crystallites these layers present a rather defective material, where mostly non-diamond inclusions populate regions in-between diamond grains. Overall, for the examined B/C range (60–60 000 ppm) and given the ultrathin character of fabricated BDD layers, the presence of non-diamond inclusions (*i.e.*, *trans* poly-acetylene, graphitic carbon) is expected, which follows our previous works on thin nanocrystalline BDD layers fabricated *via* MW-PECVD and MW-LA-PECVD techniques, while the quality of the layers can be further improved by implementing a larger thickness or higher gas-phase boron content.

Following our recent work, nanocrystalline BDD layers fabricated *via* MW-LA-PECVD surface-wave-plasma generally exhibit rather moderate electrical characteristics when compared to BDD layers synthesized *via* conventional MW-PECVD or HFCVD systems[28] In the case of the latter synthesis systems the typical process temperature at the substrate surface varies between 800–1100 °C and in some cases even above, which is a decisive factor for the incorporation of boron atoms particularly at substitutional positions into the diamond lattice which grant the p-type conductivity, overall enhancing electrical characteristics of the material. Therefore, the utilized low synthesis temperature of 500 °C (at the substrate surface) is expected to affect the incorporation of boron atoms into the layers.[28]

To examine and compare the concentration of boron in the obtained nanocrystalline BDD layers, glow discharge optical emission spectroscopy (GDOES) technique has been utilized, as it has been recently demonstrated as an effective method for determination of boron content in diamond layers[31] A typical depth profile of the nanocrystalline BDD layer characterized using GDOES is demonstrated in Fig. 6(a), where small visible oscillations of the boron (B 208 line) are attributed to the interference at the analysed layer of the incident light from the plasma and the light reflected from the substrate (Si). Additionally, a single fringe of the boron line visible in the depth profile in Fig. 6(a) corresponds to a sputtered thickness of approximately 43 nm (given the typical refractive index of diamond n = 2.4).[31] Furthermore, the corresponding volume concentrations of boron (atoms per cm^{-3}, recalculated from the GDOES) for BDD layers synthesized with various B/C ratios

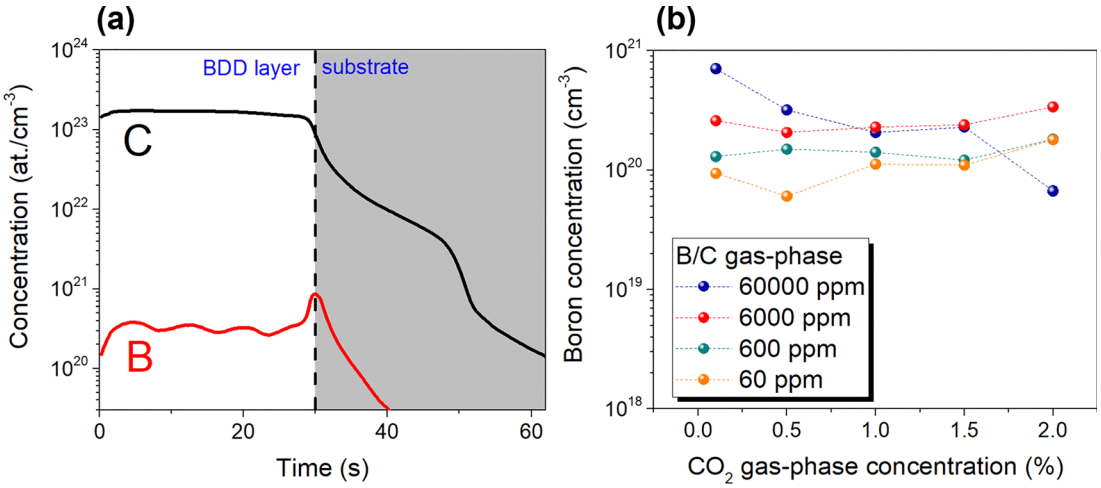

Fig. 6 (a) Concentration of boron atoms for the BDD-60k-2 sample *versus* the time of sputtering as established by GDOES, where C denotes carbon and B denotes boron. A gradual decrease of both B and C signals visible after *ca.* 30 s of sputtering is due to the interdiffusion between the BDD layer and the substrate, occurring during the synthesis process. (b) Boron concentration values for ultrathin BDD layers as a function of implemented gas-phase B/C ratio and CO_2 content.

and CO_2 levels in the gas-phase are presented on Fig. 6(b). In the case of samples prepared with B/C of 60 000 ppm the addition of CO_2 gas has a significant effect on the concentration of boron in the layers, where a decrease in the boron content with increasing CO_2 addition is clearly discernible. As expected, the BDD-60k-1 layer with 0.1% of CO_2 demonstrates the highest B concentration among all examined layers, an observation which is also supported by Raman measurements, where this layer exhibited the most pronounced shift in the diamond peak position along with the appearance of PDOS-related band (see Fig. 5). As the concentration of CO_2 in the gas-phase increases (0.5–2%), the measured boron content in the layers gradually decreases (see Fig. 5(b), BDD-60k series), which can be partially attributed to the formation of BOx species in the plasma, which do not incorporate into the diamond lattice.[26,27] For BDD series doped with B/C of 6000 ppm (samples BDD-6k-1,2,3,4,5) the change in the CO_2 content in the gas phase (0.1–2%) does not result in the significant deviation in the B concentration (Fig. 6(b)), where B concentration varies between 1.8–2 $\times$ 10^{20} cm^{-3}. At B/C ratios of 600 and 60 ppm a further decrease in the B concentration to around 1 $\times$ 10^{20} cm^{-3}, while variation of the CO_2 in the gas-phase is seen to provide a minimal effect to B incorporation at this range of B/C (Fig. 6(b)), signaling the existence of a certain threshold for the gas-phase boron concentration (*i.e.* B/C in the range of 6000 ppm) after which the effect of CO_2 addition is substantially reduced.

As the electrical properties of BDD usually present one of the main interesting properties, particularly in the context of potential applications, fabricated nanocrystalline BDD layers were further characterized and compared in terms of their electrical resistivity characteristics. Following our recent report, due to the low implemented gas-phase boron doping (B/C ratios of 60–60 000 ppm) samples are expected to display characteristics resembling a moderately doped p-type semiconductor, with the active charge carrier concentrations in the range of 10^{17} cm^{-3} (and below).[29] The BDD layers fabricated with B/C ratio of 60 000 ppm demonstrate resistivity values in the range between cca 2 and 50 Ω cm, where a visible increase in the resistivity (Fig. 7) relates to the consequent increase in CO_2 in the gas-phase, and therefore confirms the previous observations from the GDOES and Raman. It is important to note that given the low synthesis temperature of 500 °C, the incorporation of boron atoms that provide electrically active sites for conductivity within the diamond lattice is not only perturbed by the interaction between boron and oxygen species in the plasma (*i.e.*, formation of BOx complexes) but also by the passivation of boron atoms by hydrogen and therefore incorporation of electrically inactive BH complexes within the BDD layer. The formation of BH complexes has been recently investigated for BDD layers fabricated in the same synthesis system where the total boron concentration in the layers (assessed *via* secondary-ion mass spectroscopy) significantly diverged from the concentration of electrically active boron atoms incorporated into the lattice (determined from Hall effect).[28] Furthermore, for BDD layers synthesized with B/C of 6000 ppm the resistivity follows the same uptrend with the increasing CO_2 gas-phase concentration (see Fig. 7); nevertheless, the resistivity values experience a much more pronounced change from cca 90 Ω cm for BDD-6k-1 layer (0.1% of CO_2) to 11 kΩ cm for BDD-6k-5 layer (2% of CO_2). The similar behavior is observed for BDD layers fabricated with B/C of 600 and 60 ppm, where electrical resistivity increases rapidly with the increase in the CO_2 gas-phase content, while resistivity values range from cca 1.2–71 kΩ cm to 8.5–135 kΩ cm for BDD-600 and BDD-60 layers, respectively (Fig. 7). Overall, due to a combination of factors such as thin layer thickness (cca 150 nm), low synthesis temperature (*i.e.*, 500 °C) and low implemented B/C ratios (in terms of ppm concentration for MW-LA-PECVD system) the fabricated ultrathin nanocrystalline BDD layers exhibit a

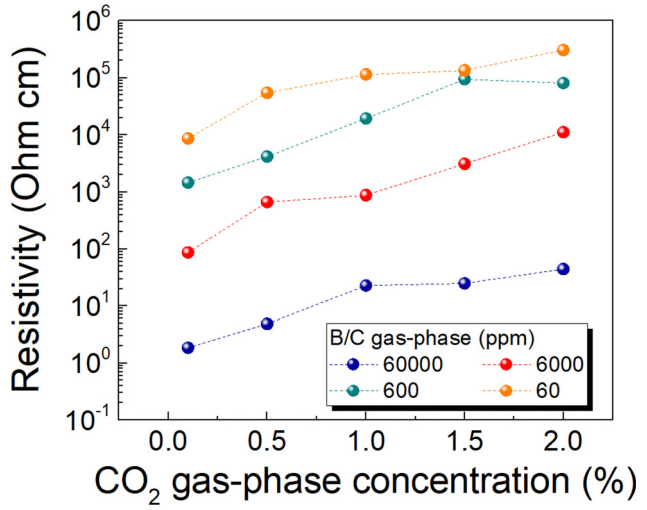

Fig. 7 Resistivity values of ultrathin BDD layers as a function of CO_2 concentration in the gas-phase for layers prepared with various B/C ratios.

semi-conductive character with regard to resistivity characteristics (*i.e.* resistivity in the order of tens of Ω cm and above), and their electrical properties may be varied by the implementation of various levels of oxygen containing gas (such as CO_2). It is worth noting that addition of oxygen gas is important in the case of MW-LA-PECVD system as it is required for the suppression of SiC formation which was previously observed and investigated.[26,27] Although, the addition of CO_2 in the gas-phase does not significantly alter the resistivity of BDD layers fabricated at B/C level of 60 000 ppm, as the concentration of boron species decreases in the plasma (B/C of 6000 ppm and below) the addition of CO_2 has a much more pronounced effect on the development of highly resistive BDD layers (*i.e.*, steeper change of resistivity values per decade seen on Fig. 7). Finally, as for certain applications the magnitude of electrical resistivity of nanocrystalline BDD layers may be required to remain in the order of mΩ cm (*i.e.*, degenerately-doped semiconductor), higher levels of B/C ratio in the gas-phase may be implemented (up to 230 000 ppm) as demonstrated in our previous works on the synthesis of highly conductive BDD layers (resistivity of cca 100 mΩ cm), therefore demonstrating versatility of the MW-LA-PECVD system for the synthesis of diamond layers/electrodes.[27–29]

To demonstrate the electrochemical behavior of ultrathin BDD layers, the Si/BDD electrodes (*i.e.*, BDD layers deposited onto conductive silicon p-type substrates) were subjected to electrochemical characterization by means of cyclic voltammetry. Fig. S6a and b demonstrate cyclic voltammograms measured on Si/BDD electrodes prepared with various B/C ratios (60 000 and 6000 ppm) and CO_2 gas-phase concentrations (0.1–2%). As all fabricated ultrathin BDD electrodes exhibited predominantly semiconductive characteristics (electrical resistivity above 10 Ω cm), the aqueous electrolyte solution (1 M KCl) remained practically free from the oxygen and hydrogen discharge in the range of applied potential from cca +1.5 V to −1.5 V (*vs.* Ag/AgCl), therefore granting Si/BDD electrodes with the potential window width of approximately 3.0 V. However, in the case of the Si/BDD electrode prepared with B/C of 60 000 ppm and 0.1% of CO_2, the onset of considerable faradaic current is visible starting at approximately −1 V *vs.* Ag/AgCl in the cathodic direction (Fig. S6a). Such a behaviour is partially attributed to the enhanced electrical characteristics of the BDD-60k-1 layer, which exhibited the lowest electrical resistivity (*i.e.*, 1.85 Ω cm) among all fabricated BDD layers (see Table 2). This observation aligns with our prior works, which established a correlation between low electrical resistivity of BDD electrodes and the increased magnitude of anodic/cathodic faradaic currents along with earlier onsets of oxygen/hydrogen evolution reactions.[28,29,35] Furthermore, an important observation on the effect of the gas-phase CO_2 concentration can be made – as the CO_2 concentration increases from 0.1 to 2% (for given B/C ratio) the magnitude of anodic/cathodic faradaic current gradually decreases (Fig. S6a and b). Similarly to the above-described observation, this effect is attributed to changes in electrical characteristics of BDD layers, as the addition of CO_2 during the synthesis is known to result in the increase of BDD layers' electrical resistivity.[27]

Further, fabricated Si/BDD electrodes were characterized using surface-sensitive $Fe(CN)_6^{3-/4-}$ redox probe to evaluate electron transfer processes.[29] Importantly, as BDD electrodes are known to possess hydrogen/oxygen surface functionalities which affect redox processes, all fabricated Si/BDD electrodes underwent an intentional anodic pre-treatment to achieve a stable electrochemical response. In the case of Si/BDD electrodes prepared with B/C of 60 000 ppm, the addition of gas-phase CO_2 resulted in the gradual increase of potential separation (ΔE_p) of anodic and cathodic peaks (Fig. 8(a)). The Si/BDD electrodes demonstrate a rather sluggish charge transfer kinetics with ΔE_p ranging from cca 550 mV (for BDD-60k-1) to cca 900 mV for (BDD-60k-5). Furthermore, for Si/BDD electrodes prepared with lower B/C ratios (*i.e.*, 6k, 600, and 60 ppm) the ΔE_p values are seen to range between cca 950 mV and cca 1200 mV depending on the boron-doping level and CO_2 gas-phase concentration (Fig. 8(b)). Overall, such low values of ΔE_p reflect a semiconductive nature of ultrathin BDD electrodes, where electrical characteristics are greatly affected not only by the utilized boron-doping level (B/C of 60–60 000 ppm) but also by the suppression of boron incorporation at higher CO_2 gas-phase concentrations (above 1%). At the same time, if faster charge transfer characteristics are required for ultrathin BDD layers/electrodes, higher boron-doping levels (*e.g.*, B/C of 230 000 ppm) can be utilised during MW-LA-PECVD synthesis to improve ΔE_p values (down to cca 120 mV).[29]

Finally, considering electrochemical electrodes based on ultrathin BDD layers it is important to note the stability of nanocrystalline BDD layers fabricated *via* MW-LA-PECVD synthesis. As documented in our prior works, extensive anodic oxidation and cathodic treatments performed on thin nanocrystalline BDD layers resulted in practically unchanged structural and electrochemical characteristics.[29,35] Particularly, the use of silicon substrates resulted in the improved adhesion of BDD layer to the underlying substrate granted by the formation

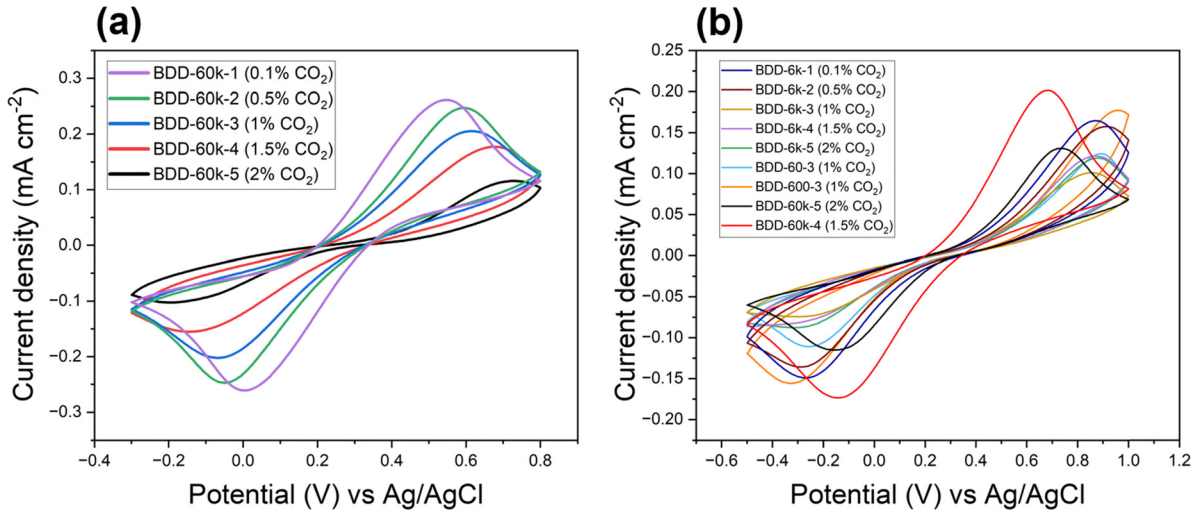

Fig. 8 Cyclic voltammograms of 1×10^{-3} M $Fe(CN)_6^{3-/4-}$ redox couple, recorded in 1 M KCl on Si/BDD electrodes. (a) Si/BDD electrodes with ultrathin BDD layer synthesized at B/C of 60k ppm, and (b) B/C of 6k, 600, and 6 ppm. Note: CV of BDD-60k-5 and BDD-60k-5 electrodes are presented for comparison.

of an interlayer (*e.g.*, silicon carbide) that is usually formed during the MW-LA-PECVD synthesis.[35] Overall, nanocrystalline BDD layers in the ultrathin form present a versatile and functional layer (*i.e.*, optically transparent, electrically conductive, electrochemically active) which can be further integrated into various advanced applications or devices that require layers/coatings exhibiting exceptional physical and chemical stability.

Considering the above, the trade-off between growth performance (*i.e.*, growth rate), BDD-coating scalability towards large areas and compatibility with temperature sensitive substrates underscores the necessity of benchmarking the SWP-synthesis approach (implemented in MW-LA-PECVD system) against conventional MW-PECVD technique to advance the synthesis of polycrystalline diamond. First, in terms of maximum deposition area and overall scalability, MW-LA-PECVD synthesis holds a clear advantage, as its design and uniform plasmas inherently facilitate large areas with the demonstration of highly homogeneous BDD-coated 6-inch wafers,[27] whereas scaling the conventional cavity-based MW-PECVD system beyond 4-inch capability yet presents an engineering challenge. Furthermore, SWP-synthesis demonstrates outstanding substrate compatibility due to depositions of diamond layers at low-temperatures (down to 100–250 °C) with proven capabilities for processing temperature-sensitive materials (*e.g.*, deposition of NCD layers on plastic substrates), making it suitable for substrates that cannot withstand the high temperatures (above 700 °C) that are typically required by conventional MW-PECVD synthesis.[23,28] Nevertheless, it is important to highlight that that conventional MW-PECVD synthesis currently outperforms SWP-approach in terms of the growth performance, achieving growth rates of typically around 500 nm h^{-1} (and above) for polycrystalline diamond compared to the much lower rates of cca 100 nm h^{-1} demonstrated for MW-LA-PECVD system. In the case of ultrathin BDD layers demonstrated in the current work, growth rates of only 25–30 nm h^{-1} were achieved; however, further fine-tuning of MW-LA-PECVD synthesis parameters and primarily a higher synthesis temperature is projected to improve the growth performance.[27] At the same time, while MW-LA-PECVD synthesis has been successfully reported to incorporate boron into diamond films in a reproducible manner demonstrating a significant effect on the electrical resistivity of BDD layers, conventional MW-PECVD synthesis still remains a more established and optimized standard for achieving high boron-doping efficiency during fabrication of polycrystalline BDD layers (often utilizing dedicated reactors for this purpose). Typical electrical resistivity values achieved for ultrathin BDD layers (cca 150 nm in thickness) fabricated *via* MW-PECVD synthesis are significantly lower (~2 mΩ cm) than the values observed for MW-LA-PECVD (~100 mΩ cm) assuming similar solid-state boron concentrations.[13,28] In conclusion, the choice of synthesis technique for polycrystalline BDD layers would ultimately depend on one's application's priority: SWP synthesis presents a promising route for large-area, low-temperature BDD coatings on diverse substrates, while MW-PECVD would be a preferred choice when the high growth rate is required whilst substrate size and synthesis temperature aspects are less constrained.

4. Conclusions

Ultrathin nanocrystalline BDD films can be readily fabricated on several industry-significant substrates (Si, glass, quartz) using surface-wave-plasma synthesis at low temperature (500 °C) in MW-LA-PECVD system. The fabricated BDD layers exhibit low thickness (of cca 150 nm) which in principle can enable conformal BDD coatings of various geometrical shapes/3D materials with resolution of several hundred nanometers and above. Further, it is demonstrated that targeting of specific

electrical properties for such BDD layers/electrodes can be achieved in a twofold manner: *via* variation of the B/C ratio in the gas-phase, or by changing the B/C ratio along with the addition of CO_2 in various concentrations. While the gas-phase concentration of the boron precursor can be changed substantially during synthesis (*i.e.*, B/C in the order of tens of ppm – to tens/hundreds of thousands ppm), the amount of CO_2 can be changed only in the limited range of concentration (in the order of 0.1–2%) without detrimental changes to layers quality. Such twofold strategy can be of significance particularly in the case when highly electrically conductive materials (*i.e.*, metals) are used as the substrate for fabrication of electrodes based on such ultrathin BDD films. In such a scenario, ultrathin BDD layers with semiconductive characteristics (resistivity in the kΩ-range) can be a preferred choice, as electrodes of certain electrical properties can be targeted, which has a particular importance in various applications where electrical properties play an essential role (*e.g.*, electrochemistry, gas-sensing, *etc.*). In terms of electrochemical characteristics, the fabricated electrodes (based on ultrathin BDD layers) demonstrated a wide window of electrochemical stability of ~2.5–3.0 V in the aqueous electrolyte, which is a comparable value reported for commonly practiced thick microcrystalline BDD electrodes. Additionally, fabricated ultrathin BDD layers exhibit very smooth surfaces (roughness of 7 nm) independently of the boron and CO_2 precursor gas-phase concentrations utilized for the synthesis, a property of very high importance specifically for optical applications of BDD films, where minimization of light scattering can be better sustained by smoother surfaces. Given the known temperature sensitivity of certain substrate materials, ultrathin BDD layers were successfully synthesized at 500 °C, overall demonstrating the suitability of the surface-wave-plasma synthesis process (and MW-LA-PECVD system in particular) for the coating of substrates with BDD films of good quality. Finally, this work presented the implementation of an advanced calculation procedure for the assessment of grain-size distribution in fabricated BDD layers, utilizing analysis of layers surfaces *via* SEM imaging, thereby providing an insight into the uniformity and consistency of the SWP synthesis process across different samples. In conclusion, ultrathin nanocrystalline BDD films emerge as a viable alternative to the conventional microcrystalline and thick BDD layers, offering similar physical characteristics while being produced through a more cost-efficient fabrication/synthesis process.

Conflicts of interest

There are no conflicts to declare.

Data availability

Raman, boron concentration, thickness/growth rate, RMS, electrochemical data, and electrical resistivity data in this manuscript is X–Y type data and is maintained by the FZU as part of the electronic laboratory library. For copies of this data contact Petr Ashcheulov (custodian). For copies of processed SEM-images contact Alexander Kovalenko (custodian of the computer code developed for analysis/image processing). There were no crystallographic databases or use of publicly available databases. Further data supporting this article (additional details on the SEM image processing and analysis; top-view SEM images; cross-section SEM; grain size distribution graphs for fabricated BDD layers; AFM images, cyclic voltammograms) is available in supplementary information (SI). See DOI: **https://doi.org/10.1039/d5ma00238a**.

Acknowledgements

This work was supported by the Czech Science Foundation (GACR) contract no. 22-04533S.

References

1 Y.-B. Park, S. Lee, M. Tobah, T. Ma and L. J. Guo, *Opt. Mater. Express*, 2023, **13**, 304–347.
2 W. Gao, J. Huang, J. He, R. Zhou, Z. Li, Z. Chen, Y. Zhang and C. Pan, *InfoMat*, 2023, **5**(8), e12426.
3 R. Haubner, *ChemTexts*, 2021, **7**, 10.
4 R. Zulkharnay and P. W. May, *Funct. Diam.*, 2024, **4**(1), 2410160.
5 N. Yang, S. Yu, J. V. Macpherson, Y. Einaga, H. Zhao, G. Zhao, G. M. Swain and X. Jiang, *Chem. Soc. Rev.*, 2019, **48**, 157–204.
6 R. J. Nemanich, J. A. Carlisle, A. Hirata and K. Haenen, *MRS Bull.*, 2014, **39**, 490–494.
7 X. Chen and W. Zhang, *Chem. Soc. Rev.*, 2017, **46**, 734–760.
8 M. Davydova, P. Kulha, A. Laposa, K. Hruska, P. Demo and A. Kromka, *Beilstein J. Nanotechnol.*, 2014, **5**, 2339–2345.
9 A. Kovalenko, P. Ashcheulov, A. Guerrero, P. Heinrichová, L. Fekete, M. Vala, M. Weiter, I. Kratochvilova and G. Garcia-Belmonte, *Sol. Energy Mater. Sol. Cells*, 2015, **134**, 73–79.
10 O. A. Williams, *Diamond Relat. Mater.*, 2011, **20**, 621–640.
11 O. Auciello and D. M. Aslam, *J. Mater. Sci.*, 2021, **56**, 7171–7230.
12 S. Handschuh-Wang, T. Wang and Y. Tang, *Small*, 2021, **17**, 2007529.
13 P. Ashcheulov, A. Taylor, J. More-Chevalier, A. Kovalenko, Z. Remeš, J. Drahokoupil, P. Hubík, L. Fekete, L. Klimša, J. Kopeček, J. Remiášová, M. Kohout, O. Frank, L. Kavan and V. Mortet, *Carbon*, 2017, **119**, 179–189.
14 S. Baluchová, A. Taylor, V. Mortet, S. Sedláková, L. Klimša, J. Kopeček, O. Hák and K. Schwarzová-Pecková, *Electrochim. Acta*, 2019, **327**, 135025.
15 M. Davydova, A. Kromka, P. Exnar, M. Stuchlik, K. Hruska, M. Vanecek and M. Kalbac, *Phys. Status Solidi A*, 2009, **206**, 2070–2073.
16 I. Kratochvílová, R. Škoda, J. Škarohlíd, P. Ashcheulov, A. Jäger, J. Racek, A. Taylor and L. Shao, *J. Mater. Process. Technol.*, 2014, **214**, 2600.

17 E. M. A. Fuentes-Fernandez, J. J. Alcantar-Peña, G. Lee, A. Boulom, H. Phan, B. Smith, T. Nguyen, S. Sahoo, F. Ruiz-Zepeda, M. J. Arellano-Jimenez, P. Gurman, C. A. Martinez-Perez, M. J. Yacaman, R. S. Katiyar and O. Auciello, *Thin Solid Films*, 2016, **603**, 62–68.
18 E. Butler and A. V. Sumant, *Chem. Vap. Deposition*, 2008, **14**, 145–160.
19 B. Baudrillart, A. S. C. Nave, S. Hamann, F. Bénédic, G. Lombardi, J. H. V. Helden, J. Röpcke and J. Achard, *Diam. Relat. Mater.*, 2017, **71**, 53–62.
20 D. Dekkar, F. Bénédic, C. Falentin-Daudré, O. Brinza, R. Issaoui and J. Achard, *Diamond Relat. Mater.*, 2019, **94**, 28–36.
21 J. Zalieckas, P. Pobedinskas, M. Møller Greve, K. Eikehaug, K. Haenen and B. Holst, *Diamond Relat. Mater.*, 2021, **116**, 108394.
22 M. Marton, M. Vojs, P. Michniak, M. Behúl, V. Rehacek, M. Pifko, Š. Stehlík and A. Kromka, *Diamond Relat. Mater.*, 2022, **126**, 109111.
23 K. Tsugawa, M. Ishihara, J. Kim, Y. Koga and M. Hasegawa, *Phys. Rev. B: Condens. Matter Mater. Phys.*, 2010, **82**, 125460.
24 J. Gu, Z. Chen, R. Li, X. Zhao, C. Das, V. Sahmuganathan, J. Sudijono, M. Lin and K. P. Loh, *Diamond Relat. Mater.*, 2021, **119**, 108576.
25 **https://sekidiamond.com/low-temperature-cvd-systems/** (accessed: August 2024).
26 A. Taylor, L. Fekete, P. Hubík, A. Jager, P. Janíček, V. Mortet, J. Mistrik and J. Vacik, *Diamond Relat. Mater.*, 2014, **47**, 27–34.
27 A. Taylor, P. Ashcheulov, P. Hubík, L. Klimša, J. Kopeček, Z. Remeš, Z. Vlčková Živcová, M. Remzová, L. Kavan, E. Scheid, J. Lorinčík and V. Mortet, *Carbon*, 2018, **128**, 164–171.
28 P. Ashcheulov, A. Taylor, Z. Vlčková Živcová, P. Hubík, J. Honolka, M. Vondráček, M. Remzová, J. Kopeček, L. Klimša, J. Lorinčik, M. Davydova, Z. Remeš, M. Kohout, A. M. Beltran and V. Mortet, *Appl. Mater. Today*, 2020, **19**, 100633.
29 P. Ashcheulov, A. Otake, K. Akai, A. Taylor, L. Klimša, P. Hubík, J. More-Chevalier and Y. Einaga, *Chem. Eng. J.*, 2023, **473**, 145463.
30 L. Pražáková, J. Fischer, A. Taylor and A. Kubíčková, *Monatsh. Chem.*, 2024, **155**, 845–850.
31 Z. Weiss, P. Ashcheulov, N. Lambert, A. Taylor, J. Lorincik, K.-D. Sung, M. Davydova and V. Mortet, *Vacuum*, 2023, **210**, 111890.
32 F. Fendrych, A. Taylor, L. Peksa, I. Kratochvilova, J. Vlcek, V. Rezacova, V. Petrak, Z. Kluiber, L. Fekete and M. Liehr, *J. Phys. D: Appl. Phys.*, 2010, **43**, 374018.
33 S. Drijkoningen, P. Pobedinskas, S. Korneychuk, A. Momot, Y. Balasubramaniam, M. K. Van Bael, S. Turner, J. Verbeeck, M. Nesládek and K. Haenen, *Cryst. Growth Des.*, 2017, **17**, 4306–4314.
34 N. Otsu, *IEEE Trans. Syst. Man Cybern.*, 1979, **9**(1), 62–66.
35 P. Ashcheulov, A. Taylor, V. Mortet, A. Poruba, F. Le Formal, H. Krýsová, M. Klementová, P. Hubík, J. Kopeček, J. Lorinčík, J.-H. Yum, I. Kratochvílová, L. Kavan and K. Sivula, *ACS Appl. Mater. Interfaces*, 2018, **10**, 29552–29564.